https://doi.org/10.5194/egusphere-2026-4506
Preprint. Discussion started: 7 August 2026

A cold-season temperature reconstruction for central Japan since 259 CE from a two-millennia Kiso *Chamaecyparis* ring-width chronology

Hitoshi Yonenobu[1], Motonari Ohyama[2], Yasuharu Hoshino[3], Genki Katata[4], Koh Yasue[5], Shin'ya Suzuki[7], Akio Nagai[1], Junpei Hirano[6], and Naoko Hasegawa[8]

[1]Graduate School of Education, Naruto University of Education, Naruto 772–8502, Japan
[2]Botanical Gardens, Tohoku University, Sendai 980–0862, Japan
[3]Nara National Research Institute for Cultural Properties, Nara 630–8577, Japan
[4]The Canon Institute for Global Studies, Tokyo 100–6511, Japan
[5]Faculty of Agriculture, Shinshu University, Minami Minowa 399–4598, Japan
[6]Department of Geography, Komazawa University, Tokyo 154–8525, Japan
[7]Faculty of Humanities and Culture, Showa Women's University, Tokyo 154–8533, Japan
[8]Faculty of Core Research, Ochanomizu University, Tokyo 112–8610, Japan

Correspondence: Hitoshi Yonenobu (yn@naruto-u.ac.jp)

Abstract. We present an annually dated reconstruction of previous November–April (pNov–Apr) temperature in central Japan from an expanded, provenance-aware Kiso *Chamaecyparis* ring-width chronology. The numerical chronology spans more than two millennia, but formal climatic interpretation is conservatively limited to 259 CE onward because replication and common-signal strength are lower and less continuous earlier. The primary model relates current-year ring-width index to a regional Chubu rural/background temperature anomaly series incorporating eight stations over 1912–2023 ($n = 112$), yielding $r = 0.416$, adjusted $R^2 = 0.165$, and RMSE $= 0.789$ °C. In seven annual split-period tests predefined in the frozen workflow, reduction of error (RE) and coefficient of efficiency (CEff) are positive in six. RE and CEff are also positive in all four formally evaluable G21 high-pass splits. No centered G21 or G51 low-pass split is formally evaluable under the leakage-safe boundary and effective-sample-size criteria; the smoothed curves are therefore used as persistence summaries rather than as independently verified low-frequency reconstructions. Synthetic tests recover an imposed 51-year signal with median $r = 0.972$, gain slope $= 0.909$, and zero median phase lag. Rule-based screening identifies two sustained G21-tail candidates: 1999–2015 CE is retained with conditional support of 1.000 and adequate interval-specific SSS, whereas 1458–1473 CE is not retained because its support is 0.744, below the 0.800 threshold. Spatial correlations and comparisons with documentary snowfall, sea-surface temperature, and circulation indices support a regional winter-climate interpretation but are not independent validation or attribution. The reconstruction provides directly tested annual and sub-21-year information together with a cautiously interpretable view of multidecadal persistence since 259 CE.

https://doi.org/10.5194/egusphere-2026-4506
Preprint. Discussion started: 7 August 2026

1 Introduction

Japan occupies the eastern, ocean-facing margin of the East Asian monsoon domain, where circulation influences associated with continental Eurasia, the western North Pacific, and the midlatitude westerlies interact through the seasonal cycle (Huang et al., 2012; Chen et al., 2019). In the warm season, the archipelago is influenced by the migration and multiscale structure of the Baiu–Meiyu frontal circulation (Ninomiya and Akiyama, 1992; Ding and Chan, 2005); in the cold season, it lies downstream of the Siberian High–Aleutian Low pressure system and of planetary-wave and teleconnection variability extending across Eurasia and the North Pacific (Takaya and Nakamura, 2013; Ma and Chen, 2021). Japan therefore records the regional expression of a coupled, multilevel monsoon system rather than the behavior of a single circulation center. Steep mountain topography further modifies these large-scale influences, producing strong regional gradients in temperature and snowfall.

Annually resolved climate reconstructions from the Japanese archipelago are valuable because they can show how this large-scale variability is expressed at the continent–ocean margin. The long history of written observation and wooden construction also provides unusually rich instrumental, documentary, archaeological, and dendrochronological archives. Central Japan is therefore well suited to testing whether an annually dated proxy can recover regional cold-season climate and be interpreted alongside other forms of evidence. Directly calibrated reconstructions remain scarce, however, particularly for the cold season, when temperature influences snowfall, snowmelt, phenology, and human activity in montane regions. A site-scale February–April reconstruction from Changbai Mountain and a later gridded December–February reconstruction based on 260 temperature-sensitive tree-ring chronologies demonstrate the potential of cold-season records at regional and continental scales (Zhu et al., 2009; Song et al., 2021). The latter also showed that reconstructed winter and summer temperature histories differed substantially in amplitude and rate of change, underscoring the value of season-specific proxy records.

Tree rings are among the few archives that can address these questions at exact calendar-year resolution. Their advantages include replication among trees and direct calibration against instrumental observations. Ring-width chronologies also present well-known challenges: age-related growth, detrending choices, changing sample depth, material selection, and seasonal covariance can all alter the climate information retained in the final chronology (e.g. Fritts, 1976; Cook and Kairiukstis, 1990). A long chronology is therefore not, by itself, a reliable climate reconstruction. Its calendar placement, replication, standardization, climate response, verification, and frequency-dependent behavior must all be evaluated explicitly.

Earlier work in central Japan established two complementary directions for long-term tree-ring climate research. A Hinoki ring-width reconstruction targeted February–April temperature and showed that ring width can preserve a late-winter to early-spring temperature signal (Yonenobu and Eckstein, 2006). A geographically distinct Korean-pine ring-width reconstruction from Changbai Mountain likewise targeted February–April temperature and compared the resulting series with East Asian winter-monsoon indices (Zhu et al., 2009). A later 2600-year oxygen- and hydrogen-isotope study extracted a summer hydroclimate component from tree-ring cellulose (Nakatsuka et al., 2020). These approaches address different climate domains. Ring width and stable isotopes need not respond to the same season, variable, or frequency band, and neither should be judged against the expectations of the other. The more useful question is which climate information each proxy supports after calibration and uncertainty are made explicit.

https://doi.org/10.5194/egusphere-2026-4506
Preprint. Discussion started: 7 August 2026

The Kiso region provides a strong basis for revisiting ring-width-based cold-season reconstruction. Kiso *Chamaecyparis* material occurs in living forests, historical buildings, archaeological contexts, and buried-wood deposits. A recently developed two-millennia chronology supplies the dated framework for the present analysis (Ohyama et al., 2026a). Related work on Nezuko or Kurobe (*Thuja standishii*) and Koyamaki (*Sciadopitys verticillata*) further demonstrates that Kiso timber archives reflect wood use, forest history, and sampling provenance as well as climate (Yonenobu et al., 2026a, b). We use an expanded version of the Kiso *Chamaecyparis* chronology, strengthened by additional living-tree material and improved overlap between modern and historical components. The chronology is treated as a material-source-aware proxy archive rather than as a simple average from a single homogeneous stand.

The instrumental target also requires careful definition. A nearby station such as Takayama provides a valuable local and historical reference, but a single record can retain effects of station history, exposure, local topography, and urbanization-related influences. Urban heat-island studies emphasize that site characteristics and urban–rural context must be documented when air-temperature records are compared (Stewart and Oke, 2012; Stewart, 2019). We therefore use the regional Chubu rural/background temperature anomaly series described by Katata et al. (2023, 2025). The product incorporates eight rural/background stations selected to reduce urbanization-related influence. Individual JMA stations remain essential for climate-response and spatial-correlation analyses. Raw Takayama and regional Chubu rural/background temperatures share strong seasonal variability. For displays requiring comparable mean levels, a season-specific additive offset places the stored Chubu anomaly series on a comparable seasonal scale. The offset leaves correlation, variance, and the ordinary least-squares slope within a specified regression direction unchanged, but the resulting mean difference depends on the chosen climatological alignment. The comparison therefore diagnoses target definition and is not a direct estimate of urban heat-island magnitude.

This study (i) documents the expanded chronology and the conservative interval adopted for climatic interpretation, (ii) fixes the pNov–Apr seasonal target and compares the regional Chubu rural/background series with a Takayama-based legacy reference, (iii) calibrates a primary RWI(t) model and tests predictor sensitivity with a constrained carry-over formulation, and (iv) evaluates annual and frequency-dependent evidence, uncertainty, sustained-interval screening, and spatial representativeness. Leakage-safe split-specific filtering provides formal out-of-sample evidence for annual and evaluable G21 high-pass variability; centered G21 and G51 low-pass components are treated as persistence summaries and assessed separately with internal signal-retention tests. Supplementary analyses provide documentary snowfall, COBE-SST2, winter-monsoon, multiresolution, and alternative-season context. Together, these analyses define both the climatic value and the limits of the Kiso cold-season reconstruction.

2 Data and methods

2.1 Tree-ring materials and chronology design

We developed the reconstruction from an expanded Kiso *Chamaecyparis* ring-width dataset. Throughout this paper, “cold season” denotes mean temperature from the previous November through April (pNov–Apr), assigned to the year containing

https://doi.org/10.5194/egusphere-2026-4506
Preprint. Discussion started: 7 August 2026

Table 1. Principal material, target, and reconstruction definitions used in the main text.

Item	Definition or value
Tree-ring archive	Kiso *Chamaecyparis* ring-width chronology
Material groups	Living trees (A–C; additional series relative to Ohyama et al. (2026a)), archaeological coffin wood from Minamimotomachi (13MM), Hachobori-sanchome (13HT), and Mirokuji-ato (13MR) as cluster D, Chiko-ji/Yakushi-do building timbers (20IK) as cluster E, a Chiko-ji/Yakushi-do bridge component (E_in_D), and Tohyama buried wood (20TY) as cluster F
Numerical chronology span	156 BCE–2025 CE; signed-year machine-readable files use -156 to 2025 and omit year 0
Formal interpretation interval	259–2025 CE under a conservative author-defined rule; the first isolated centered 51-year SSS window above 0.85 occurs at 119 CE
Primary chronology candidate	RWdiv SPL150
Primary climate target	Regional Chubu rural/background pNov–Apr mean temperature anomaly, incorporating eight rural/background stations (Katata et al., 2025)
Primary predictor	RWI(t)
Carry-over sensitivity	mean[RWI(t), RWI($t+1$)]
Authoritative calibration	1912–2023; 112 complete pNov–Apr seasons
Frequency-dependent evidence	Annual and G21 high-pass formally evaluated; centered G21 and G51 low-pass not formally evaluable and used as persistence summaries

January–April. The dataset builds on the two-millennia Kiso chronology of Ohyama et al. (2026a), but was rebuilt for climate analysis after adding living-tree material and strengthening overlap between modern and historical components.

Source material was grouped before chronology calculation so that provenance, sample history, and overlap remained explicit. Living-tree cluster A contains 259 series whose earliest measured rings postdate the 1708 forest-policy benchmark: 241 Hinoki (*Chamaecyparis obtusa*) and 18 Sawara (*C. pisifera*). Cluster B contains 43 series beginning from 1665 through 1708 (40 Hinoki and 3 Sawara), and cluster C contains 36 series beginning before 1665 (35 Hinoki and 1 Sawara). These dates are cohort indicators based on the earliest measured ring, not germination dates. Sawara represents 22 of 338 living-tree series and was combined with Hinoki because the material crossdates coherently in the regional Kiso framework; species-specific climate responses were not estimated and this remains a limitation.

Archaeological coffin wood from Minamimotomachi (13MM), Hachobori-sanchome (13HT), and Mirokuji-ato (13MR) forms cluster D. Historical building timbers from Chiko-ji/Yakushi-do (20IK) form cluster E, and Tohyama buried-forest material (20TY) forms cluster F. An additional 20IK bridge component, E_in_D, connects historical and archaeological components and is not treated as an independent material class. This grouping preserves information that would be lost by treating all samples as one spatially and historically homogeneous forest population.

https://doi.org/10.5194/egusphere-2026-4506
Preprint. Discussion started: 7 August 2026

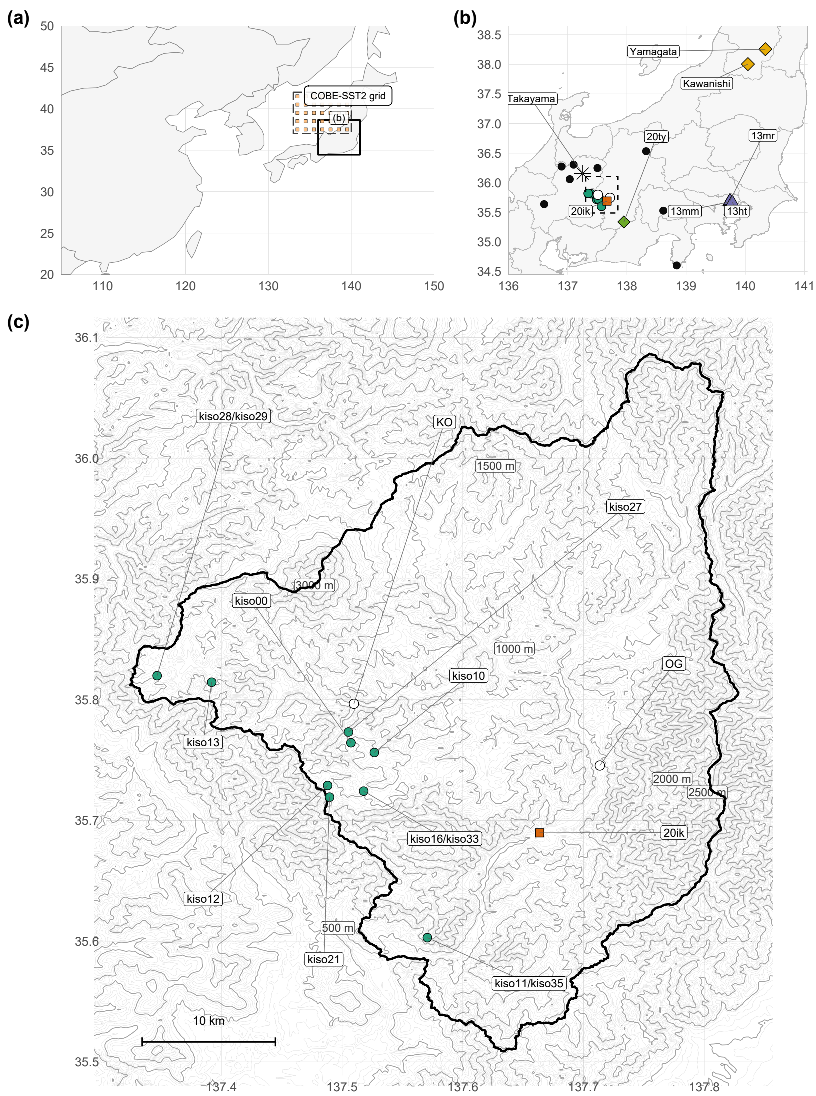

Figure 1. Study area, sampling context, and external climate-context domains. The map distinguishes the Kiso material used to construct the *Chamaecyparis* chronology from auxiliary observations used only for interpretation. JMA stations and the regional Chubu rural/background target define the instrumental temperature framework. Documentary snowfall locations and COBE-SST2 domains provide supplementary winter-climate context and are not predictors in the reconstruction model. Elevation data are from the Fundamental Geospatial Data digital elevation model of the Geospatial Information Authority of Japan; national forest-area data are from the National Land Numerical Information service of the Ministry of Land, Infrastructure, Transport and Tourism.

https://doi.org/10.5194/egusphere-2026-4506
Preprint. Discussion started: 7 August 2026

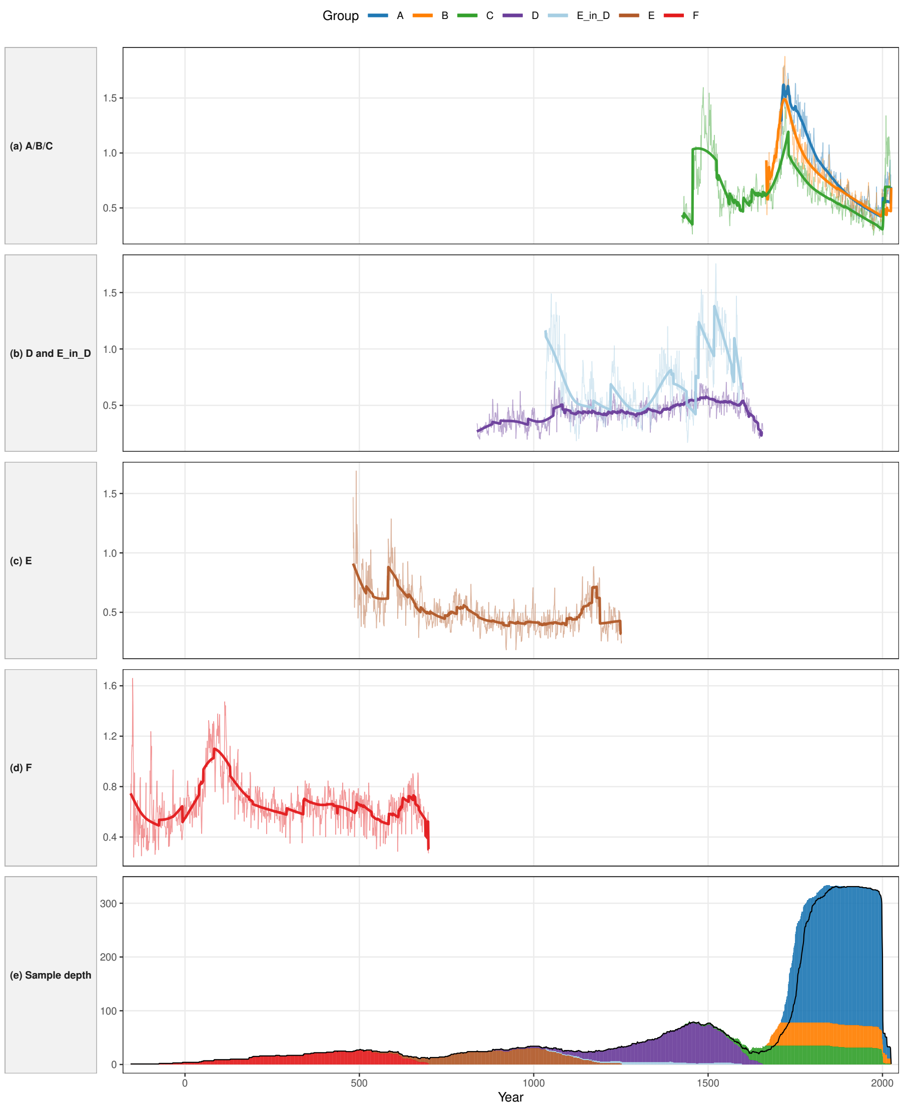

Figure 2. Raw chronology construction and sample-depth structure for the Kiso *Chamaecyparis* dataset. Panels (a)–(d) show source-group ring-width series and fitted growth curves for living-tree clusters A–C, archaeological cluster D with the E_in_D overlap component, historical-building cluster E, and buried-wood cluster F, respectively. Panel (e) shows annual sample depth by source group and for the combined chronology. The standardized chronology and running subsample signal strength are shown separately in Supplement Fig. S1.

2.2 Standardization and signal-strength assessment

Raw ring widths were converted to dimensionless ring-width indices by ratio standardization. Growth-curve form was allowed to differ among material groups because living trees, building timbers, archaeological wood, and buried wood have different

https://doi.org/10.5194/egusphere-2026-4506
Preprint. Discussion started: 7 August 2026

age structures and sampling histories (Fritts, 1976; Cook and Kairiukstis, 1990). The primary candidate is labeled RWdiv SPL150 in the supplementary files. Relevant historical, archaeological, and buried-wood components use a 150-year cubic smoothing spline, while cluster C uses a second-order polynomial bridge to 1730 CE. The polynomial is a standardization and joining device, not an ecological classification.

Standardization candidates were assessed using chronology continuity, climate response, sample depth, SSS, and synthetic signal-retention tests. Running SSS was calculated in centered 51-year windows. The numerical chronology extends from -156 to 2025. SSS $= 0.85$ is a conventional screening value rather than a physical or statistically unique threshold, and the first isolated window above it is centered at 119 CE. An analysis prioritizing maximum record length could reasonably adopt that earlier start. We instead adopted 259 CE as an author-defined, conservative boundary for formal climatic interpretation because replication and common-signal support are lower and less continuous in the earlier record. The boundary is not an estimated changepoint or a date derived from climate calibration. Values before 259 CE are retained as lower-confidence output, and annual SSS remains available for interval-specific assessment because local dips also occur after 259 CE.

2.3 Instrumental target and primary model specification

We used JMA station observations and the regional Chubu rural/background temperature anomaly series for climate-response analysis and calibration (Katata et al., 2023, 2025). The archived release initially documents 1916–2023. A subsequent update, prepared with the same eight-station rural/background framework, extends the monthly Chubu series back to 1911; the derived seasonal series used in this study are included in the restricted-review reproducibility archive with approval from the data provider. The internal identifier “chubu7” refers to Chubu’s regional number in the source classification and not to the station count. The regional product is used instead of treating one urban or local station as the climate quantity represented by the chronology. Stored monthly values use a 1940–1949 anomaly reference.

Candidate seasonal summaries include pNov–Apr, FMA, MAM, JAS, and JASO. The authoritative seasonal specification is fixed as pNov–Apr temperature, while adjacent seasons document proxy-domain sensitivity and continuity with earlier work. Predictor selection is a separate decision: the primary predictor is current-year RWI, and a constrained adjacent-ring carry-over formulation is retained as a sensitivity analysis. The alternative seasons and carry-over predictor do not select or replace the primary specification.

The updated monthly source interval begins in 1911, but pNov–Apr requires the previous November and therefore contains 112 complete seasons from 1912 through 2023 in the authoritative calibration. The primary model is

$$T_{\mathrm{anom}}(t) = \alpha + \beta\,\mathrm{RWI}(t) + \varepsilon(t),$$

where $T_{\mathrm{anom}}(t)$ is the regional Chubu rural/background pNov–Apr anomaly assigned to year t. The carry-over sensitivity uses adjacent rings to represent persistence in proxy response; it does not use future climate information. Ordinary least-squares statistics include correlation, adjusted R^2, RMSE, the Durbin–Watson statistic, and residual AR1.

https://doi.org/10.5194/egusphere-2026-4506
Preprint. Discussion started: 7 August 2026

2.4 Annual and frequency-dependent verification

Annual out-of-sample behavior was evaluated with seven predefined calibration–verification splits. For each split, the model was fitted only in the calibration segment and applied unchanged to the verification segment. Reported statistics include verification correlation, RMSE, reduction of error (RE), coefficient of efficiency (CEff), sign agreement, and effective sample size. CEff is used for coefficient of efficiency to avoid confusion with Common Era dates.

Frequency-dependent verification was recomputed with a leakage-safe design. Calibration and verification segments were filtered independently. Centered G21 and G51 kernels were not allowed to cross a split boundary, incomplete transformed edge values were excluded, and formal evaluation required complete transformed support and a Bretherton effective sample size of at least eight (Bretherton et al., 1999) ($n_{\mathrm{eff}} \geq 8$). Annual and G21 high-pass results can therefore be evaluated in at least some splits. A low-pass scale with no formally evaluable split is reported as not evaluable; it is not assigned a verification statistic and is not used to claim low-frequency predictive skill. Smoothed G21 and G51 reconstruction curves are retained as persistence summaries and are assessed separately by synthetic signal-retention and standardization-robustness tests.

2.5 Uncertainty and reconstruction products

The production uncertainty workflow (method u2.0) uses 2000 bootstrap draws. It combines calibration-parameter uncertainty with weighted selection among four predefined chronology-standardization members. Conditional-mean draws represent uncertainty in the fitted reconstruction; predictive draws additionally include moving-block resampling of calibration residuals with a primary block length of five years. The uncertainty scope does not include source-group removal, species exclusion, or individual-series resampling, and these omitted components should not be inferred from the reported intervals. No calibration-only fallback was used.

The reconstructed series is stored on the 1940–1949 anomaly scale. The authoritative calibration period ends in 2023. Values for 2024 and 2025 are retained as out-of-calibration predictions and are excluded from calibration, verification, and interval screening. For displays requiring absolute temperature, an additive offset based on the 1991–2020 station climatology can be applied. This conversion changes the plotted level but not regression coefficients, verification statistics, uncertainty widths, or interval ranking. All anomalies quoted for reconstructed intervals remain on the stored 1940–1949 scale.

2.6 Rule-based sustained-interval screening

Sustained candidates were identified from the centered G21 conditional-mean reconstruction between 259 CE and the last complete G21 center year, 2015. The 10th and 90th percentiles define lower- and upper-tail years. Internal gaps of at most three years were bridged, and intervals shorter than 15 years were excluded. G51, which ends in 2000, is descriptive only and never determines selection or retention.

For each fixed point-estimate candidate, conditional support is the fraction of conditional-mean bootstrap draws for which the mean over that same interval remains beyond the draw-specific G21 threshold. Retention requires conditional support of at least 0.800 and adequate replication. Primary replication support uses centered 51-year SSS windows that cover at least 80 %

https://doi.org/10.5194/egusphere-2026-4506
Preprint. Discussion started: 7 August 2026

of the candidate interval. At least three windows are required and none may fall below SSS $= 0.85$. SSS is never interpolated annually. Center-year-within-interval assignment is retained only as a non-decisional comparison. All candidates are reported together with their decision; fallback and top-N replacement are prohibited.

2.7 Spatial and external climate context

Spatial representativeness was evaluated using JMA station temperatures and CRU TS land-air temperature. Correlations characterize the geographic footprint of the calibrated reconstruction but are not independent validation because the fields belong to the same instrumental climate system used to define the target. Documentary snowfall ratios, COBE-SST2, and published winter circulation indices were compared with the reconstruction as external context. These comparisons were not used in calibration or model selection and do not establish causal attribution. Smoothing-dependent associations are reported descriptively because serial dependence reduces effective sample size.

3 Results

3.1 Chronology structure and signal strength

The final Kiso *Chamaecyparis* chronology is assembled from overlapping material groups rather than from one homogeneous stand (Fig. 2). Living trees connect the chronology to the instrumental period, while archaeological wood, historical building timbers, and buried wood extend it backward. The usable climate record therefore depends on overlap and common-signal strength, not simply on the oldest ring.

The numerical chronology uses signed calendar years, extends from -156 to 2025, and reaches a maximum sample depth of 331 series. Running SSS has a mean of 0.884 and a maximum of 0.995, but it is much lower in the earliest, sparsely replicated portion. The first isolated centered 51-year window above SSS $= 0.85$ occurs at 119 CE. Formal climatic interpretation nevertheless begins in 259 CE under the conservative author-defined rule adopted above. Because neither the SSS criterion nor the 259 CE boundary represents an objective changepoint, the complete SSS series is retained for interval-specific assessment.

3.2 Primary target, calibration, and verification

The authoritative target is the regional Chubu rural/background pNov–Apr temperature anomaly, assigned to the year containing January–April. The public target incorporates eight stations. Several adjacent seasonal windows correlate positively with ring width; these comparisons document proxy-domain sensitivity rather than select a replacement primary reconstruction. FMA remains a bridge to the earlier reconstruction (Yonenobu and Eckstein, 2006), and other seasons are supplementary comparisons.

Predictor choice was evaluated separately. The primary RWI(t) calibration covers 1912–2023 and contains 112 complete seasons. It gives $r = 0.416$, $R^2 = 0.173$, adjusted $R^2 = 0.165$, and RMSE $= 0.789$ °C. The Durbin–Watson statistic is 1.777

https://doi.org/10.5194/egusphere-2026-4506
Preprint. Discussion started: 7 August 2026

Table 2. Authoritative calibration and leakage-safe verification summary for the primary pNov–Apr model and the constrained carry-over sensitivity. Full-period calibration covers 1912–2023 ($n = 112$). Annual values summarize seven calibration–verification splits predefined in the frozen analysis workflow. G21 high-pass values use independently filtered calibration and verification segments; low-pass G21 and G51 results are not formally evaluable and are therefore not assigned predictive-skill statistics.

Model	Full-period calibration	Annual split verification	G21 high-pass verification	Interpretation
Primary RWI(t)	$r = 0.416$; adjusted $R^2 = 0.165$; RMSE $= 0.789\,°C$; DW $= 1.777$; AR1 $= 0.045$	RE and CEff positive in 6/7 splits; mean RE $= 0.175$; mean CEff $= 0.099$; minimum CEff $= -0.068$	4/7 splits evaluable; RE and CEff positive in 4/4; mean CEff $= 0.127$; median verification $r = 0.341$	Authoritative reconstruction
Carry-over mean[RWI(t), RWI($t+1$)]	$r = 0.368$; adjusted $R^2 = 0.128$; RMSE $= 0.807\,°C$; DW $= 1.824$; AR1 $= 0.024$	RE and CEff positive in 5/7 splits; mean RE $= 0.030$; mean CEff $= -0.062$; minimum CEff $= -0.703$	4/7 splits evaluable; RE and CEff positive in 4/4; mean CEff $= 0.049$; median verification $r = 0.214$	Sensitivity only

and residual AR1 is 0.045. A constrained carry-over sensitivity model is weaker over the same period ($r = 0.368$, adjusted $R^2 = 0.128$, RMSE $= 0.807\,°C$), supporting the simpler current-ring predictor.

Seven annual calibration–verification splits predefined in the frozen analysis workflow were evaluated. For the primary model, RE and CEff are positive in six of seven splits. Mean RE is 0.175, mean CEff is 0.099, median verification r is 0.376, and the minimum CEff is -0.068. The annual result is therefore useful but not uniformly positive in every split. The carry-over model has positive RE and CEff in five splits and mean CEff $= -0.062$.

3.3 Regional-target comparison

Raw Takayama and regional Chubu rural/background temperatures share a strong regional signal but differ in mean level, amplitude, and error structure. In the direct comparison, the regional anomaly series was placed on a comparable seasonal temperature scale by an additive offset. This alignment does not alter correlation, variance, the OLS slope for a fixed regression direction, or regression-residual RMSE when an intercept is fitted. The displayed mean difference and regression intercept depend on the chosen alignment. The result is therefore interpreted as a target-definition comparison, not as a unique attribution of the difference to urbanization.

The legacy FMA experiment provides a like-for-like example. The Takayama blended-extension model for 1900–1961 and the regional Chubu rural/background model for 1911–1961 have almost identical calibration correlations ($r = 0.405$ and 0.406). The regional target reduces RMSE from 1.416 to 1.040 °C, changes positive CEff support from 0 of 5 to 2 of 5 splits, and raises mean CEff from -0.844 to -0.045. Its advantage is lower error and less negative out-of-sample behavior, not a larger proxy–climate correlation.

https://doi.org/10.5194/egusphere-2026-4506
Preprint. Discussion started: 7 August 2026

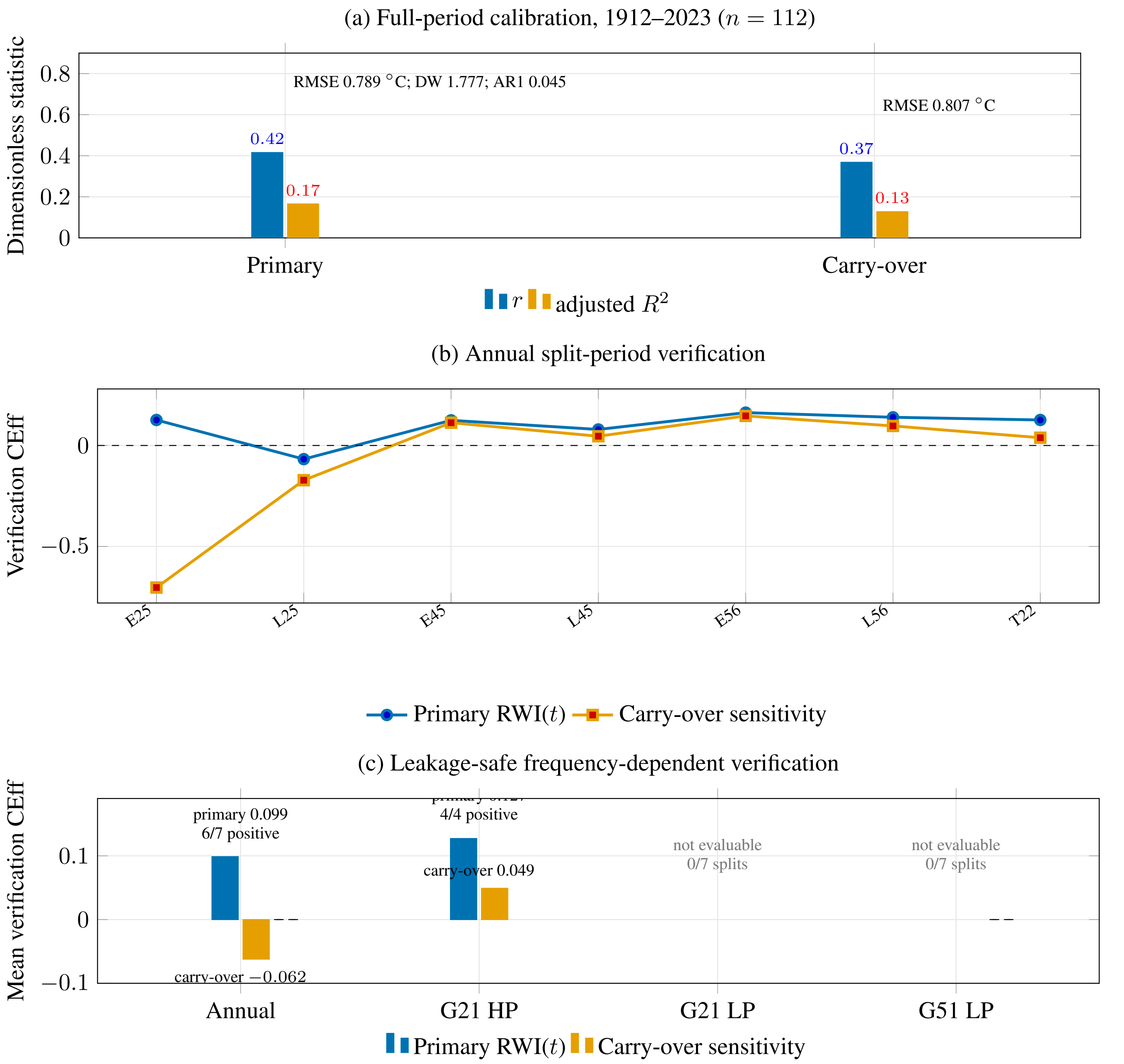

Figure 3. Calibration and verification evidence for the authoritative pNov–Apr specification. Panel (a) compares full-period calibration statistics for the primary RWI(t) model and the constrained carry-over sensitivity. Panel (b) shows annual CEff for seven prespecified splits. E25 and L25 denote the two directions of the 25-year 1912–1961 split; E45 and L45 denote the two directions of the 45-year 1912–2001 split; E56 and L56 denote the two directions of the 56-year 1912–2023 split; T22 verifies 2002–2023 from a 1912–2001 calibration. Panel (c) summarizes leakage-safe frequency-dependent verification. Calibration and verification segments were filtered independently, and low-pass results are not reported as predictive skill because no split met the formal effective-sample-size requirement.

https://doi.org/10.5194/egusphere-2026-4506
Preprint. Discussion started: 7 August 2026

3.4 Frequency-dependent evidence and signal retention

Frequency-dependent verification filtered calibration and verification segments independently. Centered kernels did not cross split boundaries, incomplete transformed edge values were excluded, and formal evaluability required $n_{\text{eff}} \geq 8$. The annual scale is evaluable in all seven splits, with positive CEff in six. G21 high-pass behavior is evaluable in four splits, and all four have positive RE and CEff; mean CEff is 0.127 and median verification r is 0.341.

No G21 low-pass or G51 low-pass split passes the combined support, boundary, and effective-sample-size requirements. These bands therefore have no formal out-of-sample verification result. G21 and G51 are retained as persistence summaries, not as independently verified low-pass reconstructions.

Synthetic input–recovery tests address whether the chronology workflow retains imposed slow signals. Median recovery correlations are 0.988, 0.986, 0.983, and 0.972 for 11-, 21-, 31-, and 51-year inputs. At 51 years, median gain slope is 0.909 and median phase lag is zero. Signals at 75–101 years are more attenuated, and recovery weakens substantially at 150–200 years. These tests support broad multidecadal timing and shape while arguing against precise centennial amplitude or stable long-period cycles.

3.5 Primary pNov–Apr reconstruction

Figure 4 shows the primary reconstruction on the stored 1940–1949 anomaly scale. The authoritative calibration period ends in 2023; values for 2024 and 2025 are out-of-calibration predictions and are not used in calibration, verification, or interval screening. The interval before 259 CE is shown for chronological continuity but is excluded from formal climatic interpretation. Running SSS remains time-varying after 259 CE, so the annual SSS record should be consulted when evaluating any particular interval.

The annual reconstruction contains substantial year-to-year variability. G21 and G51 curves are included to display persistence over decadal and multidecadal time scales, but they have different evidential roles. Annual and G21 high-pass behavior can be evaluated by leakage-safe split-period tests. Centered G21 and G51 low-pass split tests are not formally evaluable after support, boundary, and effective-sample-size screening, and the smoothed curves are therefore treated as descriptive summaries rather than as independently verified low-frequency reconstructions. Synthetic input–recovery tests show that an imposed 51-year signal is recovered with median $r = 0.972$, gain slope $= 0.909$, and zero median phase lag, supporting use of G51 for broad timing and shape while retaining caution about amplitude and external validation.

https://doi.org/10.5194/egusphere-2026-4506
Preprint. Discussion started: 7 August 2026

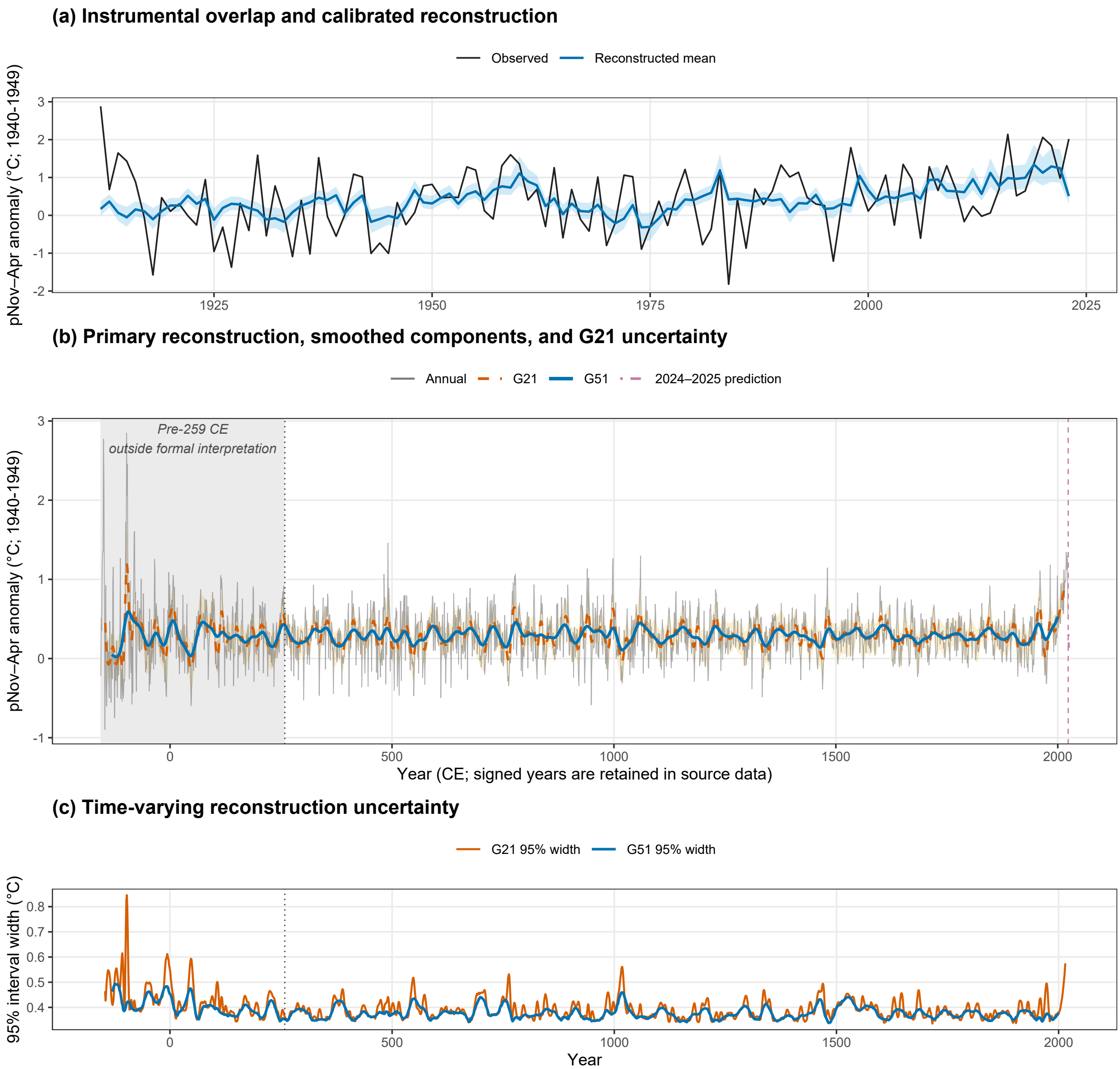

Figure 4. Primary pNov–Apr temperature reconstruction for central Japan on the stored 1940–1949 anomaly scale. Panel (a) compares the observed regional Chubu rural/background target with the reconstructed mean over the authoritative 1912–2023 calibration period; the gray band is the conditional-mean 95 % uncertainty interval. Panel (b) shows the annual reconstruction and centered G21 and G51 persistence summaries, together with the G21 conditional-mean interval. The gray background precedes the author-defined formal interpretation boundary at 259 CE. The vertical dashed line marks the calibration endpoint in 2023; 2024–2025 are shown only as out-of-calibration predictions and are excluded from calibration, verification, and interval screening. Panel (c) shows the time-varying widths of the G21 and G51 conditional-mean 95 % intervals. Predictive intervals additionally include resampled residual variability and are provided in the machine-readable products.

https://doi.org/10.5194/egusphere-2026-4506
Preprint. Discussion started: 7 August 2026

Table 3. Rule-based sustained G21-tail candidates and screening decisions for the regional Chubu pNov–Apr temperature reconstruction. Anomalies are relative to the stored 1940–1949 target baseline. Conditional support is the fraction of conditional-mean bootstrap draws in which the fixed point-estimate interval remains beyond its draw-specific G21 threshold. Primary replication support requires at least three centered 51-year SSS windows that each cover at least 80 % of the candidate interval, with no selected window below SSS $= 0.85$. G51 is descriptive only and does not determine retention.

Tail	Interval	Mean G21 anomaly, °C (conditional-mean 95 % uncertainty interval)	Conditional support	Primary SSS windows	G51 descriptor	Decision and reason
Lower-tail G21	1458–1473 CE	0.07 [−0.13, 0.33]	0.744	$n = 8$; minimum 0.927; pass	0.17 [−0.01, 0.40]	Not retained: conditional support < 0.800
Upper-tail G21	1999–2015 CE	0.68 [0.47, 0.90]	1.000	$n = 3$; minimum 0.993; pass	Not complete for the full interval (2/17 yr)	Retained calibration-era feature: all primary criteria passed

3.6 Rule-based sustained intervals

Candidate intervals were identified only from the G21 reconstruction over the formal selection domain, which ends in 2015 because a centered 21-year estimate requires complete support. The 10th- and 90th-percentile thresholds are 0.145 and 0.457 °C, respectively. After requiring a minimum duration of 15 years and bridging internal gaps of no more than three years, two candidates remain (Table 3). All candidates are shown; no fallback or top-N replacement was used.

The lower-tail candidate spans 1458–1473 CE. Its mean G21 anomaly is 0.071 °C, with a conditional-mean 95 % interval of −0.128 to 0.332 °C. Eight centered 51-year SSS windows cover at least 80 % of the candidate interval, and their minimum SSS is 0.927. The replication criterion is therefore satisfied. Conditional support is only 0.744, however, below the required 0.800, so the interval is not retained. The "lower-tail" label denotes its rank within the G21 distribution and does not require an anomaly below zero relative to the 1940–1949 target baseline.

The upper-tail candidate spans 1999–2015 CE. Its mean G21 anomaly is 0.677 °C, with a conditional-mean 95 % interval of 0.467 to 0.901 °C. Conditional support is 1.000. Three centered 51-year SSS windows, centered in 1989, 1994, and 1999, cover at least 80 % of the candidate interval; the minimum SSS is 0.993. This interval satisfies both primary criteria and is retained. A complete centered G51 estimate is available for only 2 of its 17 years because G51 ends in 2000, so no full- interval G51 descriptor is reported and G51 does not enter the decision.

https://doi.org/10.5194/egusphere-2026-4506
Preprint. Discussion started: 7 August 2026

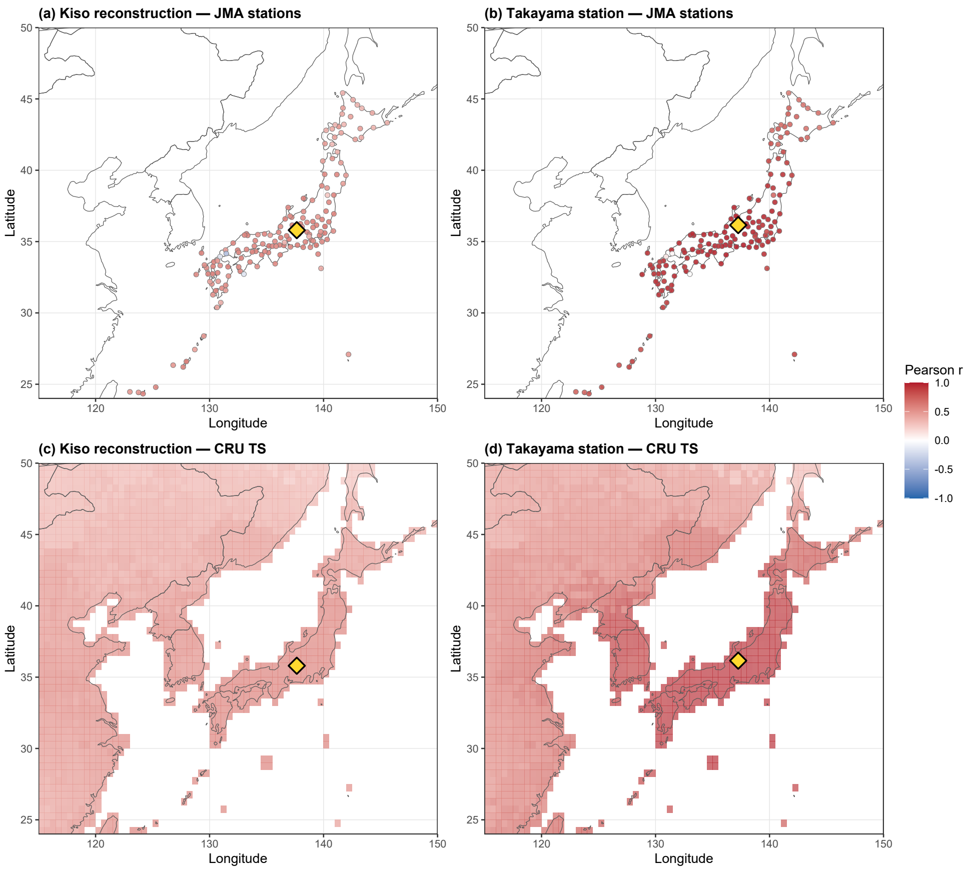

Figure 5. Spatial correlations for the Kiso reconstruction and the Takayama instrumental benchmark. Panels (a) and (b) show station-wise Pearson correlations with JMA pNov–Apr temperatures; symbol color gives the correlation coefficient, and all accepted stations are plotted with a common symbol size. No interpolated field is displayed for the JMA station panels. Panels (c) and (d) show grid-cell correlations with CRU TS pNov–Apr land-air temperature for the Kiso reconstruction and Takayama, respectively. The CRU TS panels provide broad spatial context and are not treated as independent validation.

3.7 Spatial correlation pattern over Japan and East Asia

The Kiso reconstruction correlates with a broad cold-season temperature pattern across Japan and East Asian land areas (Fig. 5). Among 151 JMA stations passing the minimum-overlap screen, the mean pNov–Apr correlation is 0.496, the median is 0.537, and the maximum is 0.643. Ninety-eight stations have $r \geq 0.5$, and six have $r \geq 0.6$. The largest accepted-station correlations occur at Tsukuba/Tateno ($r = 0.643$), Kobe (0.636), Oshima (0.631), Aikawa (0.609), Hikone (0.602), and Tsu (0.602). The mean detrended station correlation is lower (0.305), indicating that both interannual and shared slower variation contribute to the raw spatial pattern.

https://doi.org/10.5194/egusphere-2026-4506
Preprint. Discussion started: 7 August 2026

The nearby Takayama instrumental benchmark is stronger, as expected, with mean and median station correlations of 0.858 and 0.916. It is a direct temperature series, whereas the Kiso reconstruction additionally contains biological-response, chronology-standardization, and calibration noise. The relevant proxy result is the persistence of a coherent positive regional pattern, not equality with the instrumental benchmark.

For CRU TS over 1902–2023, the Kiso pNov–Apr reconstruction has a mean grid-cell correlation of 0.440, a median of 0.436, and a maximum of 0.613 over the analyzed land area. Takayama gives a stronger pNov–Apr field (mean $r = 0.569$; median 0.552; maximum 0.955). CRU TS therefore characterizes spatial plausibility and geographic context rather than independent reconstruction skill.

4 Discussion

4.1 Target definition and regional calibration

The reconstruction should be interpreted specifically as pNov–Apr temperature, not as annual temperature or a general climate index. The pNov–Apr window is the authoritative seasonal specification because it provides a broad, physically interpretable cold-season target with long instrumental coverage; neighboring seasonal windows are retained to document proxy-domain sensitivity. This target-season decision is distinct from predictor selection. The current-year RWI(t) predictor remains primary because its annual calibration and predefined split-period behavior are better than those of the constrained carry-over sensitivity. Neither decision is justified by maximizing a single calibration correlation.

A plausible biological interpretation is that late-autumn through spring conditions influence snowpack, soil temperature, cambial reactivation, frost risk, and stored resources available when growth begins (Fritts, 1976; Song et al., 2021). Korean pine at Changbai Mountain also shows a positive February–April temperature response (Zhu et al., 2009). These are regional precedents and possible pathways, not direct physiological evidence that Kiso *Chamaecyparis* responds uniformly to every month from November through April. The defensible inference is statistical: the composite cold-season target gives a reproducible regional calibration.

The regional Chubu rural/background target reduces dependence on the history of one local station. It incorporates eight rural/background stations selected to reduce urbanization-related influence (Katata et al., 2023, 2025). Takayama remains an important benchmark and the basis of the legacy FMA reconstruction, but its urban setting, station history, exposure, elevation, and local topography need not represent the forest climate recorded by the chronology. Strong Takayama–Chubu correlation shows that the regional target is not an unrelated replacement. Differences in mean level, amplitude, and error structure are consistent with the design of the rural/background product, but this comparison does not isolate urban heat-island effects from station composition, elevation, exposure, climatological alignment, or other target-definition differences. The additive alignment used for direct displays does not change correlation, variance, or regression slope within a specified direction; mean differences are conditional on that alignment and are not interpreted as urban-bias estimates.

The FMA legacy experiment illustrates the scope of this benefit. Replacing the Takayama blended-extension target with rural Chubu leaves the calibration correlation nearly unchanged but substantially lowers RMSE and makes mean CEff less

https://doi.org/10.5194/egusphere-2026-4506
Preprint. Discussion started: 7 August 2026

negative. The improvement is therefore expressed through error and out-of-sample behavior rather than a larger proxy–climate correlation. It is a specific comparison and not proof that the rural target improves every season or model.

4.2 Evidence hierarchy across time scales

Chronology signal strength and reconstruction skill answer different questions. SSS describes how closely the available sample approximates a population chronology, whereas climate skill also depends on target definition, standardization, predictor choice, calibration, and time scale (Fritts, 1976; Cook and Kairiukstis, 1990; Cook and Pederson, 2011). The 259 CE boundary is therefore a conservative workflow decision, not a physical discontinuity. Local SSS values remain necessary when interpreting individual intervals.

The leakage-safe verification results require a more restricted hierarchy of evidence than a conventional smooth-then-split analysis. Annual behavior is evaluable in seven splits and gives positive RE and CEff in six. G21 high-pass behavior is evaluable in four splits and is positive in all four. These results support useful annual and sub-21-year information, although one annual split has slightly negative CEff and three G21 high-pass splits are not evaluable.

No G21 low-pass or G51 low-pass split satisfies both boundary guards and the formal effective-sample-size criterion. The instrumental record is too short to support those centered smooths within the predefined split design without leakage or very small effective samples. We therefore do not describe G21 low-pass or G51 as out-of-sample verified bands. The smoothed curves remain useful for displaying persistence in the reconstructed series, provided that they are distinguished from independent verification.

Synthetic input–recovery tests provide complementary, internal evidence. They show that the standardization workflow preserves the timing and most of the amplitude of imposed signals through 51 years, with median 51-year recovery $r = 0.972$, gain slope 0.909, and no median phase shift. Longer signals are increasingly attenuated. This supports cautious description of multidecadal shape and timing but not precise centennial amplitude, stable cycles, or solar forcing. The conclusion is deliberately asymmetric: the tests show that the workflow can retain an imposed slow signal, but they do not establish that an observed slow feature is climatic or externally forced.

The weaker carry-over model and the close persistence of broad reconstruction features under the alternative predictor indicate that the main narrative is not created by the exact adjacent-ring formulation. The simpler RWI(t) model is retained because its annual calibration and split-period behavior are better. Any carry-over terminology refers to response persistence and does not introduce future climate information.

4.3 Rule-based intervals and the modern upper-tail feature

The revised interval screen separates candidate identification from retention. G21 thresholds, duration, and gap rules identify all sustained candidates. Bootstrap conditional support and interval-specific SSS then determine whether a candidate is retained. This architecture avoids presenting a ranked list of apparently important intervals when uncertainty or replication does not support them.

https://doi.org/10.5194/egusphere-2026-4506
Preprint. Discussion started: 7 August 2026

The 1458–1473 CE lower-tail candidate satisfies the replication rule: eight 51-year SSS windows cover at least 80 % of the interval and all exceed 0.85. Its conditional support is 0.744, however, and it is therefore not retained. This distinction is important. The result does not imply that chronology quality is poor in the interval; it means that the reconstructed G21 tail classification is not sufficiently stable across conditional-mean uncertainty draws. Historical interpretation of this candidate should consequently remain outside the primary conclusions.

The 1999–2015 CE upper-tail interval is retained. Its conditional support is 1.000, and three overlapping 51-year SSS windows have a minimum SSS of 0.993. The decision is not based on the center years alone; requiring windows to cover most of the candidate removes the artificial endpoint penalty produced by a center-year-within-interval rule. A full-interval G51 descriptor is unavailable because centered G51 ends in 2000, but G51 is explicitly non-decisional. The retained interval is therefore evidence for a sustained upper-ranked modern feature on the stored 1940–1949 anomaly scale, not a claim based on complete 51-year smoothing or an attribution of recent warming.

The positive G21 value of the lower-tail candidate is not contradictory. “Lower-tail” and “upper-tail” refer to positions within the reconstructed G21 distribution. Zero refers to the 1940–1949 target baseline. Tail ranking and the sign of an anomaly relative to that historical baseline answer different questions.

4.4 Spatial representativeness

The station analysis indicates that the reconstruction contains a regional cold-season temperature signal rather than a strictly local one. Most accepted JMA stations have positive correlations, and the median correlation is 0.537. The Takayama instrumental benchmark is much stronger, as expected, because the proxy includes biological response, chronology standardization, and calibration error. The appropriate test is whether a coherent regional pattern survives those sources of noise, not whether the proxy equals a direct instrumental series.

Detrending reduces the mean station correlation from 0.496 to 0.305. Both interannual covariance and shared slower variation therefore contribute to the raw spatial footprint. CRU TS extends the positive pattern over East Asian land areas. Because CRU and JMA are instrumental products related to the target climate system, they provide geographic plausibility rather than independent validation.

The broad pattern is physically consistent with the East Asian winter monsoon, in which continental pressure, coastal northerlies, the East Asian trough, the upper-level jet, and North Pacific circulation interact (Takaya and Nakamura, 2013; Miao and Wang, 2020; Ma and Chen, 2021). Such consistency does not establish attribution. It supports interpreting Kiso as a downstream central- Japan cold-season temperature record embedded in a larger circulation system.

4.5 Documentary snowfall, ocean conditions, and circulation context

Documentary snowfall, ocean, and circulation comparisons are not part of model calibration. Snowfall ratios in the Takeda Gen’emon diary have an established winter-climate interpretation (Hirano et al., 2012, 2025). Their local bridge to instrumental Yamagata temperature and snowfall is stronger than their direct association with Kiso, which is expected because the records

https://doi.org/10.5194/egusphere-2026-4506
Preprint. Discussion started: 7 August 2026

represent different regions and variables. They provide contextual agreement, not an independent quantitative validation of the reconstruction.

COBE-SST2 associations generally become larger after smoothing, especially in the Japan Sea and western North Pacific. The stronger association of Japanese rural/background temperature with large-scale sea-surface-temperature variability reported by Katata et al. (2025) provides additional motivation for reading these relationships as regional background- climate context. Comparable responses in control domains, however, argue against a unique Japan Sea mechanism. Smoothing also increases serial dependence and lowers effective sample size. We therefore treat the ocean coefficients as descriptive air–sea covariance, not as independent validation, significance-tested causal effects, or evidence of oceanic forcing.

The published East Asian winter monsoon index has a moderate inverse G21 association with Kiso, while a reconstructed Siberian High index alone has weak direct correspondence. This contrast is plausible because the winter monsoon is a multi-component circulation system whose centers of action need not vary coherently at all time scales (D'Arrigo et al., 2005b, a; Panagiotopoulos et al., 2005; Jeong et al., 2011; Ma and Chen, 2021). Kiso should not be described as a direct reconstruction of the Siberian High or any single circulation index.

4.6 Seasonal complementarity and limitations

The reconstruction complements the central-Japan isotope record of Nakatsuka et al. (2020), which primarily represents summer hydroclimate. The proxies differ in material, target variable, season, and time-scale response. Kiso also complements the gridded East Asian winter-temperature reconstruction of Song et al. (2021), which has broader spatial coverage but shorter temporal extent and a different network design. Neither record is an independent validation of the other.

Several limitations define the appropriate scope of inference. The primary calibration has adjusted $R^2 = 0.165$, so most annual target variance remains unexplained. One of seven annual splits has slightly negative CEff, and only four of seven G21 high-pass splits are formally evaluable. No G21 or G51 low-pass split is formally evaluable. The chronology combines living trees, archaeological wood, historical timbers, and buried wood with different source histories and selection pathways; it is not a random sample from one forest. The living chronology contains a small Sawara component, and species-specific climate sensitivity was not modeled. The uncertainty ensemble covers calibration parameters and four predefined standardization variants but not source-group removal, species exclusion, or individual-series resampling. The formal start at 259 CE is an author-defined conservative reporting rule rather than an objective changepoint, and the retained 1999–2015 CE interval lies within the calibration era.

Finally, the regional spatial fields, documentary records, SSTs, and circulation indices are contextual. The study does not claim stable cycles, solar forcing, precise centennial amplitude, a general solution to the divergence problem, or causal attribution of the retained modern interval. Its central conclusion is narrower: a provenance-aware Kiso chronology supports an annually dated pNov–Apr reconstruction since 259 CE, with useful annual verification, positive G21 high-pass behavior where evaluable, and cautiously interpretable multidecadal persistence supported by signal-retention tests.

https://doi.org/10.5194/egusphere-2026-4506
Preprint. Discussion started: 7 August 2026

5 Conclusions

We used an expanded, provenance-aware Kiso *Chamaecyparis* ring-width chronology to reconstruct regional pNov–Apr temperature in central Japan. The numerical chronology extends from -156 to 2025, but formal climatic interpretation conservatively begins in 259 CE. This is an author-defined reporting boundary rather than an estimated changepoint or a date derived from climate calibration. The authoritative calibration period ends in 2023; values for 2024 and 2025 are out-of-calibration predictions and are not used for calibration, verification, or interval screening.

The primary RWI(t) model covers 112 complete seasons from 1912 through 2023 and gives $r = 0.416$, adjusted $R^2 = 0.165$, and RMSE $= 0.789$ °C. Annual RE and CEff are positive in six of seven predefined split tests, and both statistics are positive in all four formally evaluable G21 high-pass splits. No G21 or G51 low-pass split is formally evaluable after leakage-safe boundary guards and effective-sample-size screening. The smoothed curves are therefore persistence summaries, not independently verified low-frequency reconstructions.

Synthetic input–recovery tests retain 11–51-year signals well. At 51 years, median recovery correlation is 0.972, gain slope is 0.909, and median phase lag is zero. This supports cautious interpretation of broad multidecadal timing and shape, but not precise centennial amplitude, stable cycles, or external forcing.

Rule-based G21 screening identifies two sustained candidates. The 1458–1473 CE lower-tail candidate has adequate interval-specific SSS but is not retained because conditional support is 0.744, below the 0.800 threshold. The 1999–2015 CE upper-tail interval is retained because conditional support is 1.000 and the interval-specific SSS criterion is satisfied. This result identifies a robust upper-ranked calibration-era feature on the stored 1940–1949 anomaly scale; it is not independent pre-instrumental validation and does not constitute causal attribution of recent warming.

The regional Chubu rural/background target reduces dependence on one station history, while spatial analyses show a coherent cold-season footprint across Japan and East Asian land areas. Documentary snowfall, ocean-temperature, and circulation comparisons provide physically plausible winter-climate context but are not independent validation. The reconstruction complements summer hydroclimate records from central Japan and provides directly tested annual and sub-21-year information together with a transparent, cautiously interpretable record of multidecadal persistence since 259 CE.

6 Supplementary material

The Supplement provides chronology and SSS diagnostics, annual and leakage-safe frequency-dependent verification, synthetic signal-retention tests, carry-over sensitivity, descriptive smoothed-mean contrasts, multiresolution products, documentary snowfall and SST/circulation context, and the Takayama–rural Chubu target comparison. It distinguishes formally evaluable out-of-sample tests from non-evaluable low-pass diagnostics and documents the complete Table 3 v5.3 candidate, uncertainty, and SSS-window audit.

https://doi.org/10.5194/egusphere-2026-4506
Preprint. Discussion started: 7 August 2026

Code and data availability. The provenance information and mean curves needed to evaluate chronology dating are available with Ohyama et al. (2026a); the associated public chronology dataset is archived by Ohyama et al. (2026b). The methods and background for the regional Chubu rural/background temperature product are described by Katata et al. (2025). The corresponding 1916–2023 monthly dataset is archived by Katata and Fujibe (2026). A subsequent update extends the same eight-station monthly framework back to 1911. The data provider approved inclusion of the derived seasonal series used for the 1912–2023 pNov–Apr calibration and the supplementary target comparison in the restricted-review archive.

A password-protected reviewer copy of the frozen reproducibility archive is available through Tohoku University at https://nc.rdx.tohoku.ac.jp/s/AcPZEpWR2fHsz5L. The access password is provided separately to the editor and is not printed in the manuscript. Upon acceptance, the archive will be preserved in the Tohoku University institutional research-data repository and assigned a DOI; the final article will cite that DOI in place of the temporary review link.

The archive provides the final annual ring-width index used as the primary predictor, the year-aligned regional Chubu rural/background target data used for calibration, the reconstructed temperature series, conditional-mean and predictive uncertainty products, annual and leakage-safe frequency-dependent verification outputs, running SSS, signal-retention summaries, spatial and target-comparison products, Table 3 v5.3 audit outputs, and figure source data. It also provides the R, Python, and PowerShell code, validation tests, data dictionaries, manifests, checksums, and session information required to reproduce all manuscript-facing climate analyses from the finalized chronology onward. Original analysis code is released under the MIT License; author-created data and derived products are released under CC BY 4.0. Provider-derived files retain their provider-specific terms, documented file by file in the archive metadata.

Full annual documentary-derived Kawanishi series and full annual D'Arrigo circulation-index values are not redistributed because their redistribution terms were not established for this release. Source publications and provider records should be consulted for those values. Derived correlations, synthesis tables, figure-source products that do not reproduce the excluded annual series, and validation records are included where redistribution permits.

Individual raw ring-width measurement series are not included in the present release. Their material provenance and dating context, together with mean curves suitable for chronology assessment, are documented by Ohyama et al. (2026a) and the associated dataset cited above. Species-resolved living-tree measurements are being curated with their metadata for companion research. The accompanying repository reproduces all reported climate analyses from the finalized annual RWI onward, but it does not reproduce construction of that RWI from the individual measurement series. Requests for specific non-public measurements may be directed to the corresponding author and will be considered subject to coauthor agreement, provenance constraints, and completion of related studies.

Analyses were conducted in R (R Core Team, 2025). The chronology-development and climate-analysis workflows used `dplR` (Bunn, 2008; Bunn et al., 2025), `tidyverse`, `zoo`, `ggplot2`, `patchwork`, `sf`, `terra`, and `ncdf4`. External data sources, versions, access dates, licenses, and disclosure status are documented in the repository metadata. Elevation data in Fig. 1 were obtained from the Fundamental Geospatial Data digital elevation model of the Geospatial Information Authority of Japan, and national forest-area data from the National Land Numerical Information service. JMA station observations came from the agency's historical data service. The regional Chubu rural/background temperature product is described by Katata et al. (2023, 2025); COBE-SST2 by Hirahara et al. (2014); and CRU TS v4.09 by Harris et al. (2020).

Author contributions. HY: conceptualization, data curation, formal analysis, funding acquisition, investigation, methodology, project administration, resources, software, supervision, validation, visualization, writing – original draft, and writing – review and editing. MO: data

https://doi.org/10.5194/egusphere-2026-4506
Preprint. Discussion started: 7 August 2026

curation, formal analysis, funding acquisition, investigation, project administration, resources, validation, and writing – review and editing. YH: data curation, formal analysis, funding acquisition, investigation, resources, validation, and writing – review and editing. GK: data curation, formal analysis, validation, and writing – review and editing. KY: data curation, validation, and writing – review and editing. SS: data curation, investigation, resources, and writing – review and editing. AN: data curation, investigation, validation, and writing – review and editing. JH: conceptualization, data curation, formal analysis, validation, and writing – review and editing. NH: data curation, funding acquisition, resources, and writing – review and editing.

Competing interests. The authors declare that they have no conflict of interest.

Acknowledgements. We thank the Kiso District Forest Service and the Kiso Kanzai Ichiuri Cooperative for permission to photograph market logs. We also acknowledge the organizations that maintain the elevation, forest-area, station, gridded temperature and sea-surface-temperature datasets used in this study. We thank Rosanne D'Arrigo of the Lamont-Doherty Earth Observatory of Columbia University for providing the reconstructed Siberian High and East Asian winter monsoon index data. ChatGPT (OpenAI) was used as an assistive tool for English-language editing and for identifying and debugging problems in R and shell scripts. No AI-generated data or analyses were used. All scientific claims, calculations, interpretations, and code changes were independently checked and approved by the authors, who take full responsibility for the manuscript.

Financial support. This study was supported by JSPS KAKENHI Grant Numbers 25K00544 to Hitoshi Yonenobu, 24K04405 to Junpei Hirano, 25H00503 to Yasuharu Hoshino, 20H01368, 24K00152, and 24K21370 to Motonari Ohyama, 24H00118 to Naoko Hasegawa, and 24K04414 to Genki Katata.

https://doi.org/10.5194/egusphere-2026-4506
Preprint. Discussion started: 7 August 2026

References

Bretherton, C. S., Widmann, M., Dymnikov, V. P., Wallace, J. M., and Bladé, I.: The Effective Number of Spatial Degrees of Freedom of a Time-Varying Field, Journal of Climate, 12, 1990–2009, https://doi.org/10.1175/1520-0442(1999)012<1990:TENOSD>2.0.CO;2, 1999.

Bunn, A., Korpela, M., Biondi, F., Campelo, F., Mérian, P., Qeadan, F., Zang, C., Buras, A., Cecile, A., Mudelsee, M., Schulz, M., Klesse, S., Frank, D., Visser, R., Cook, E., and Anchukaitis, K.: dplR: Dendrochronology Program Library in R, https://CRAN.R-project.org/package=dplR, last accessed: July 29, 2026, 2025.

Bunn, A. G.: A Dendrochronology Program Library in R (dplR), Dendrochronologia, 26, 115–124, https://doi.org/10.1016/j.dendro.2008.01.002, 2008.

Chen, W., Wang, L., Feng, J., Wen, Z., Ma, T., Yang, X., and Wang, C.: Recent progress in studies of the variabilities and mechanisms of the East Asian monsoon in a changing climate, Advances in Atmospheric Sciences, 36, 887–901, https://doi.org/10.1007/s00376-019-8230-y, 2019.

Cook, E. R. and Kairiukstis, L. A.: Methods of Dendrochronology: Applications in the Environmental Sciences, Kluwer Academic Publishers, Dordrecht, ISBN 9780792305867, https://doi.org/10.1007/978-94-015-7879-0, 1990.

Cook, E. R. and Pederson, N.: Uncertainty, emergence, and statistics in dendrochronology, in: Dendroclimatology: Progress and prospects, edited by Hughes, M., Swetnam, T., and Diaz, H. F., chap. 4, pp. 77–112, Springer, https://doi.org/10.1007/978-1-4020-5725-0, 2011.

D'Arrigo, R., Jacoby, G., Wilson, R., and Panagiotopoulos, F.: A reconstructed Siberian High index since A.D. 1599 from Eurasian and North American tree rings, Geophysical Research Letters, 32, L05 705, https://doi.org/10.1029/2004GL022271, 2005a.

D'Arrigo, R., Wilson, R., Panagiotopoulos, F., and Wu, B.: On the long-term interannual variability of the East Asian winter monsoon, Geophysical Research Letters, 32, L21 706, https://doi.org/10.1029/2005GL023235, 2005b.

Ding, Y. and Chan, J. C. L.: The East Asian summer monsoon: an overview, Meteorology and Atmospheric Physics, 89, 117–142, https://doi.org/10.1007/s00703-005-0125-z, 2005.

Fritts, H. C.: Tree Rings and Climate, Academic Press, London, ISBN 9780122684500, 1976.

Harris, I., Osborn, T. J., Jones, P., and Lister, D.: Version 4 of the CRU TS monthly high-resolution gridded multivariate climate dataset, Scientific Data, 7, 109, https://doi.org/10.1038/s41597-020-0453-3, 2020.

Hirahara, S., Ishii, M., and Fukuda, Y.: Centennial-scale sea surface temperature analysis and its uncertainty, Journal of Climate, 27, 57–75, https://doi.org/10.1175/JCLI-D-12-00837.1, 2014.

Hirano, J., Ohba, T., Morishima, W., and Mikami, T.: Reconstruction of winter temperature since the 1830s in Kawanishi based on historical weather documents, Geographical Review of Japan Series A, 85, 275–286, in Japanese with English abstract, 2012.

Hirano, J., Hasegawa, N., Zaiki, M., and Mikami, T.: Long-term variations of snowfall ratio in the Sea of Japan side area of the Tohoku region since the late 17th century, Journal of Geography (Chigaku Zasshi), 134, 429–438, https://doi.org/10.5026/jgeography.134.429, in Japanese with English abstract, 2025.

Huang, R., Chen, J., Wang, L., and Lin, Z.: Characteristics, processes, and causes of the spatio-temporal variabilities of the East Asian monsoon system, Advances in Atmospheric Sciences, 29, 910–942, https://doi.org/10.1007/s00376-012-2015-x, 2012.

Jeong, J.-H., Ou, T., Linderholm, H. W., Kim, B.-M., Kim, S.-J., Kug, J.-S., and Chen, D.: Recent recovery of the Siberian High intensity, Journal of Geophysical Research: Atmospheres, 116, D23 102, https://doi.org/10.1029/2011JD015904, 2011.

Katata, G. and Fujibe, F.: Monthly Background/Rural Air Temperature Data in Japan (1916–2023), https://doi.org/10.24567/0002006246, [data set], 2026.

Katata, G., Connolly, R., and O'Neill, P.: Evidence of Urban Blending in Homogenized Temperature Records in Japan and in the United States: Implications for the Reliability of Global Land Surface Air Temperature Data, Journal of Applied Meteorology and Climatology, 62, 1095–1114, https://doi.org/10.1175/JAMC-D-22-0122.1, 2023.

Katata, G., Nakayama, R., Fujibe, F., and Maeda, S.: Reconstruction of the Background Air Temperature Record in Japan (1916–2023): Implications for Climate Change and Urbanisation Bias in the 20th Century, International Journal of Climatology, 45, e70 141, https://doi.org/10.1002/joc.70141, 2025.

Ma, T. and Chen, W.: Climate variability of the East Asian winter monsoon and associated extratropical–tropical interaction: a review, Annals of the New York Academy of Sciences, 1504, 44–62, https://doi.org/10.1111/nyas.14620, 2021.

Miao, J. and Wang, T.: Decadal variations of the East Asian winter monsoon in recent decades, Atmospheric Science Letters, 21, e960, https://doi.org/10.1002/asl.960, 2020.

Nakatsuka, T., Sano, M., Li, Z., Xu, C., Tsushima, A., Shigeoka, Y., Sho, K., Ohnishi, K., Sakamoto, M., Ozaki, H., Higami, N., Nakao, N., Yokoyama, M., and Mitsutani, T.: A 2600-year summer climate reconstruction in central Japan by integrating tree-ring stable oxygen and hydrogen isotopes, Climate of the Past, 16, 2153–2172, https://doi.org/10.5194/cp-16-2153-2020, 2020.

Ninomiya, K. and Akiyama, T.: Multi-scale features of Baiu, the summer monsoon over Japan and the East Asia, Journal of the Meteorological Society of Japan. Ser. II, 70, 467–495, https://doi.org/10.2151/jmsj1965.70.1B_467, 1992.

Ohyama, M., Yonenobu, H., Hoshino, Y., and Suzuki, S.: A two-millennia provenance-assured Chamaecyparis tree-ring chronology for central Japan, Dendrochronologia, 95, 126 461, https://doi.org/10.1016/j.dendro.2025.126461, 2026a.

Ohyama, M., Yonenobu, H., Hoshino, Y., and Suzuki, S.: Tree-ring_chronology_CJH25, https://doi.org/10.50974/0002007851, [data set], 2026b.

Panagiotopoulos, F., Shahgedanova, M., Hannachi, A., and Stephenson, D. B.: Observed trends and teleconnections of the Siberian High: A recently declining center of action, Journal of Climate, 18, 1411–1422, https://doi.org/10.1175/JCLI3352.1, 2005.

R Core Team: R: A Language and Environment for Statistical Computing, R Foundation for Statistical Computing, Vienna, Austria, https://www.R-project.org/, 2025.

Song, M., Yang, B., Ljungqvist, F. C., Shi, F., Qin, C., and Wang, J.: Tree-ring-based winter temperature reconstruction for East Asia over the past 700 years, Science China Earth Sciences, 64, 872–889, https://doi.org/10.1007/s11430-020-9768-9, 2021.

Stewart, I. D.: Why should urban heat island researchers study history?, Urban Climate, 30, 100 484, https://doi.org/10.1016/j.uclim.2019.100484, 2019.

Stewart, I. D. and Oke, T. R.: Local Climate Zones for Urban Temperature Studies, Bulletin of the American Meteorological Society, 93, 1879–1900, https://doi.org/10.1175/BAMS-D-11-00019.1, 2012.

Takaya, K. and Nakamura, H.: Interannual variability of the East Asian winter monsoon and related modulations of the planetary waves, Journal of Climate, 26, 9445–9461, https://doi.org/10.1175/JCLI-D-12-00842.1, 2013.

Yonenobu, H. and Eckstein, D.: Reconstruction of early spring temperature for central Japan from the tree-ring widths of Hinoki cypress and its verification by other proxy records, Geophysical Research Letters, 33, https://doi.org/10.1029/2006gl026170, 2006.

Yonenobu, H., Nagai, A., Ohyama, M., and Hoshino, Y.: A ring-width reference chronology of Nezuko/Kurobe (Thuja standishii (Gordon) Carrière, Cupressaceae) from the Kiso Mountains, central Japan, Japanese Journal of Historical Botany, 35, 35–44, 2026a.

Yonenobu, H., Ohyama, M., Hoshino, Y., Nagai, A., and Aoyagi, T.: Dendrochronology of *Sciadopitys verticillata* (Koyamaki) in central Japan: radial-growth patterns and climate response, Dendrochronologia, 98, 126 565, https://doi.org/10.1016/j.dendro.2026.126565, 2026b.

https://doi.org/10.5194/egusphere-2026-4506
Preprint. Discussion started: 7 August 2026

Zhu, H. F., Fang, X. Q., Shao, X. M., and Yin, Z. Y.: Tree ring-based February–April temperature reconstruction for Changbai Mountain in Northeast China and its implication for East Asian winter monsoon, Climate of the Past, 5, 661–666, https://doi.org/10.5194/cp-5-661-2009, 2009.